Electrocatalysis

Deutsche Ausgabe: DOI: 10.1002/ange.201702332
Internationale Ausgabe: DOI: 10.1002/anie.201702332

# The Effect of Surface Site Ensembles on the Activity and Selectivity of Ethanol Electrooxidation by Octahedral PtNiRh Nanoparticles

*Nina Erini, Vera Beermann, Martin Gocyla, Manuel Gliech, Marc Heggen, Rafal E. Dunin-Borkowski, and Peter Strasser**

***Abstract:*** *Direct ethanol fuel cells are attractive power sources based on a biorenewable, high energy-density fuel. Their efficiency is limited by the lack of active anode materials which catalyze the breaking of the C–C bond coupled to the 12-electron oxidation to $CO_2$. We report shape-controlled PtNiRh octahedral ethanol oxidation electrocatalysts with excellent activity and previously unachieved low onset potentials as low as 0.1 V vs. RHE, while being highly selective to complete oxidation to $CO_2$. Our comprehensive characterization and in situ electrochemical ATR studies suggest that the formation of a ternary surface site ensemble around the octahedral $Pt_3Ni_1Rh_x$ nanoparticles plays a crucial mechanistic role for this behavior.*

The conversion of ethanol in direct ethanol fuel cells (DEFCs) directly into electrical energy has been widely examined in recent years.[1] Ethanol is considered a green fuel since it can be produced from biomass and offers high volumetric and gravimetric energy density (8 kWh kg$^{-1}$), good energy efficiency, and easy handling, storage and transportation, in contrast to gaseous fuels.[2] The ethanol oxidation reaction (EOR), however, is often incomplete due to difficulties in C–C bond cleavage, resulting in a number of byproducts other than $CO_2$. Alkaline medium in the fuel cell presents several advantages when compared to acidic medium, like faster kinetics for the oxygen reduction on the cathodic counterpart and a broader range of non-noble co-catalysts.[3] Alloying Pt with highly oxophilic transition metals has been a promising strategy to modify the electrocatalytic surface properties of Pt in order to supply active oxygen-containing species, such as OH, which readily oxidize adsorbed molecular fragments while reducing the cost of the catalyst considerably.[4]

[*] Dr. N. Erini, V. Beermann, M. Gliech, Prof. P. Strasser
The Electrochemical Energy, Catalysis, and Materials Science Laboratory, Department of Chemistry, Chemical Engineering Division, Technical University Berlin
10623 Berlin (Germany)
E-mail: pstrasser@tu-berlin.de
M. Gocyla, Dr. M. Heggen, Dr. R. E. Dunin-Borkowski
Ernst Ruska-Centre for Microscopy and Spectroscopy with Electrons, Forschungszentrum Juelich GmbH
52425 Juelich (Germany)
Prof. P. Strasser
Ertl Center for Electrochemistry and Catalysis, Gwangju Institute of Science and Technology
Gwangju 500-712 (South Korea)

Supporting information for this article can be found under: https://doi.org/10.1002/anie.201702332.

The combination of Pt with Rh and Ni in a single-phased spherical nanoscaled electrocatalyst proved to be highly promising for the EOR.[5] Even higher electrocatalytic activities and stabilities are to be expected for polyhedral shapes in comparison to their unshaped counterparts, since polyhedral surface facets provide better preconditions for the formation of ordered active surface site ensembles.[6] Electrocatalytic properties and the reactivity of nanoparticles are directly related to their surface structure and shape. Perfect Pt (111) planes are known to show no formation of poisonous CO species, unless they show defects or steps, but earlier onset potentials for $CO_2$ formation in comparison with other Pt basal planes.[7] In order to elucidate the beneficial shape-controlling effects for electrocatalysts, a novel electrocatalytic system comprising octahedral Pt-Ni-Rh with fixed Pt:Ni ratios and different Rh contents ($Pt_3Ni_1Rh_x$-oct/C) in the form of supported nanoparticles with {111} facets were prepared using a wet-chemical approach with metal carbonyls present during the reduction process and a mixture of oleylamine and oleic acid as solvents, where $x$ was varied between the equivalent of 1 and 6 atomic %. The bulk composition of the resulting PtNiRh-1/C, PtNiRh-3/C and PtNiRh-6/C was controlled by adjusting the initial Pt, Ni and Rh precursor ratios. The high Pt content was chosen to ensure sufficient active surface site formation and to determine the influence of changes in the minimal amounts of Rh in terms of selectivity to different ethanol oxidation pathways. The bulk composition and metal loading, which were determined by inductively coupled plasma (ICP) optical spectroscopy, proved to be close to the desired nominal values (see Table S1 in the Supporting Information). Transmission electron microscopy (TEM) images of the electrocatalysts (Figure S1) show that in all three samples the nanoparticles were well distributed across the carbon support and largely regular octahedral in shape, enclosed by eight {111} facets. Mean edge lengths, which were estimated from TEM and derived edge length histograms inserted in the TEM images in Figure S1 and listed in Table S1, vary in a narrow range from $7.2 \pm 1.1$ nm to $8.0 \pm 1.0$ nm. The higher magnification images reveal a lattice spacing of 0.23 nm, which can be attributed to Pt fcc (111) in all samples. An additional lattice spacing of 0.19 nm in samples PtNiRh-1/C and PtNiRh-6/C can be attributed to Pt fcc (200).

Figure 1 a–c shows atomic-scale high angle annular dark field scanning TEM (HAADF/STEM) images of the different $Pt_3Ni_1Rh_x$-oct/C catalyst nanoparticles after the first EOR cycle, approximately oriented along ⟨110⟩, with octahedral morphologies. Figure 1 d–i shows corresponding energy dispersive X-ray spectroscopy (EDX) composition maps. For all

  

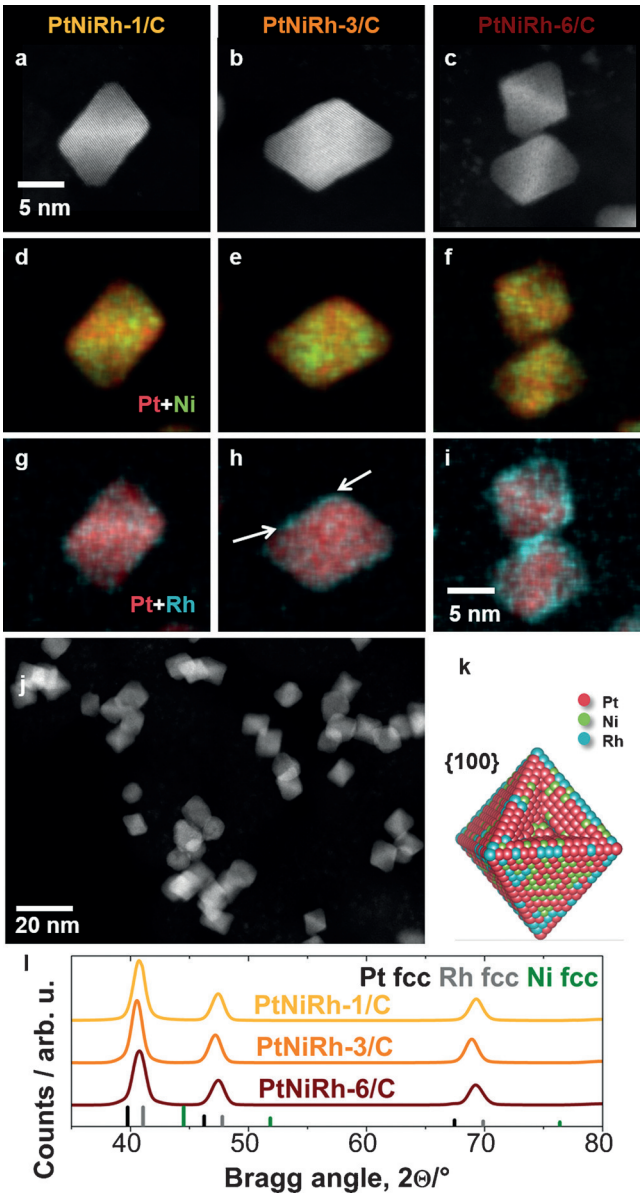


***Figure 1.*** a–c,j) HAADF-STEM images and d–i) EDX composition map analysis after the first EOR scan of PtNiRh-1/C (a,d,g), PtNiRh-3/C (b,e,h) and PtNiRh-6/C (c,f,i) octahedral nanoparticles oriented close to ⟨110⟩. j) Overview HAADF-STEM image of PtNiRh-6/C. d–f) EDX composition map showing the distribution of Pt (red) and Ni (green) and g–i) Pt (red) and Rh (blue), respectively. k) Schematic of the Rh-rich shell and mixed Ni, Rh and Pt core. l) Cu $K_\alpha$ XRD pattern of the three $Pt_3Ni_1Rh_x$-oct/C electrocatalysts shown alongside the expected peak positions for pure fcc Pt, pure fcc Rh and pure fcc Ni, indicated using black, gray and green lines, respectively.

nanoparticles and compositions, the EDX maps confirm an enrichment of Ni at the facets and the presence of a Pt-rich frame, which can be identified by a Pt-rich strip in the center of each particle (Figure 1 d–f). The Pt and Ni elemental distribution in each particle corresponds to that reported in earlier work.[8] Shape-selective nanocatalysts offer activity benefits based on structural sensitivity and high surface area. We recently demonstrated that octahedral PtNi nanoparticle catalysts show exceptional oxygen reduction activity gain over state-of-the-art unshaped Pt electrocatalysts.[9]

EDX composition maps for PtNiRh-1/C nanoparticles with the lowest Rh content show a speckled distribution of Rh over the nanoparticle, which gives rise to isolated Rh-rich patches (Figure 1 g). With a higher Rh content for PtNiRh-3/C, an accumulation of Rh at the surfaces of the octahedral particles is observed (Figure 1 h, highlighted by arrows). For PtNiRh-6/C, the particles with the highest Rh content, the EDX maps indicate the formation of a compact Rh-rich shell around each octahedral particle (Figure 1 i). The formation of a compact Rh-rich shell is more obvious for slightly smaller nanoparticles (Figure S2). HAADF/STEM images acquired before the first EOR scan are shown in Figure S3 and an overview over all samples is given in Figure S4. The compositions of the individual particles in Figure 1, measured using EDX are $Pt_{71}Ni_{25}Rh_4$, $Pt_{72}Ni_{23}Rh_5$ and $Pt_{66}Ni_{23}Rh_{11}$, respectively, in close agreement with the ICP results for the bulk samples. The EDX composition maps indicate that the Pt and Ni distribution is the same as after the first EOR scan, that is, they indicate the formation of Ni-rich facets and a Pt-rich frame in each particle. This means that the nanocatalysts, which are uniform in size and shape, show good tolerance towards the reaction conditions. In a previous study we could show, that this class of Rh-doped Pt-Ni octahedral nanoparticles proved to be stable in shape for electrochemical reaction conditions up to 30000 cycles, making this material a promising candidate for the application in DEFCs.[6b]

The fitted X-ray diffraction (XRD) powder patterns of all $Pt_3Ni_1Rh_x$-oct/C specimens show relatively broad Bragg peaks, typical for nano-sized particles with limited structural coherence (Figure 1 l). There are no superlattice peaks discernible below $2\theta = 35°$, indicating a substitutional solid solution alloy. All of the electrocatalysts show a single-phase face centered cubic diffraction pattern, as also revealed by the lattice spacing visible in micrographs. The diffraction peaks are consistent with an atomic mixture of the three metals, as they occur between the reflections expected for Pt, Rh and Ni. No reflections for pure metallic Pt, Rh or Ni are observed, indicating alloy formation for all three compositions. However, as a result of the slightly asymmetric diffraction peaks of the $Pt_3Ni_1Rh_x$-oct/C catalysts, the presence of a second fcc phase cannot be completely excluded. The theoretical $2\theta_{theo}$ values listed in Table S2, which are derived from the atomic ratio of Pt:Ni from ICP results (Table S1), are in good agreement with the experimental $2\theta_{exp}$ values for all of the samples and (*hkl*) reflections.

The catalytic activity of the $Pt_3Ni_1Rh_x$-oct/C electrocatalysts for ethanol electrooxidation in alkaline media was evaluated in order to correlate the catalyst structure and composition with electrocatalytic EOR polarization behavior. Figure 2 a shows the specific activity of the electrocatalysts in alkaline media: PtRhNi-3/C has the highest forward anodic peak of $13.6 \pm 0.9\ mA\ cm_{ECSA}^{-2}$, nearly as high as that for PtNiRh-1/C with $12.0 \pm 0.2\ mA\ cm_{ECSA}^{-2}$ and almost double than that for PtNiRh-6/C with $6.9 \pm 0.1\ mA\ cm_{ECSA}^{-2}$ (summary of the electrochemical values is presented in Table S3). The decrease in the onset anodic potential indicates an enhancement in the kinetics of the ethanol oxidation reaction

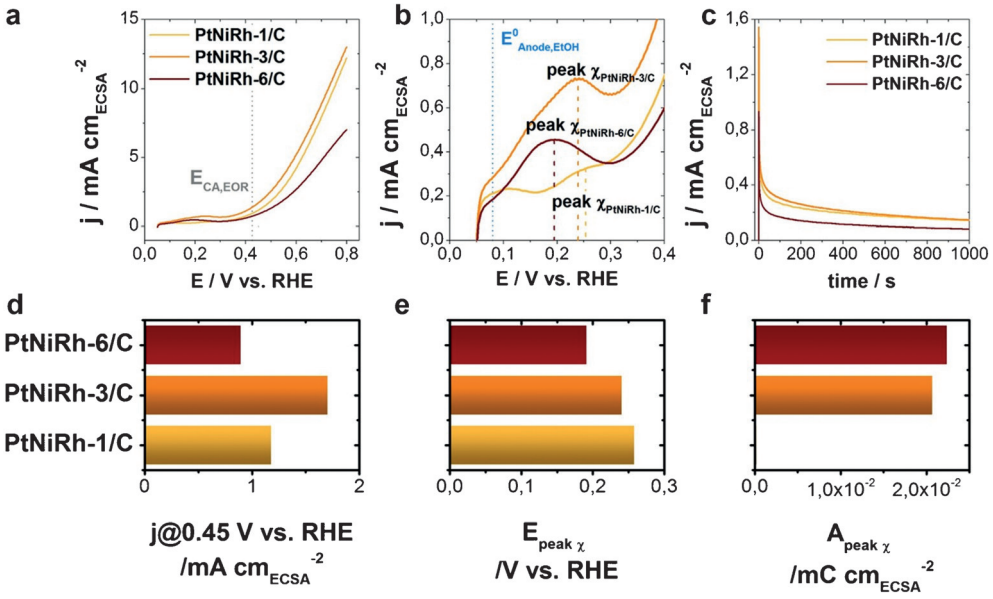


***Figure 2.*** a,b) First forward scan with a scan rate of 20 mV s$^{-1}$ and c) potentiostatic chronoamperometry at 0.45 V vs. RHE of the ethanol oxidation reaction (EOR) on the three $Pt_3Ni_1Rh_x$-oct/C electrocatalysts in 0.1 M KOH containing 0.5 M ethanol. Current densities are normalized by ECSA. The vertical gray dashed line marks the potential used for the chronoamperometric experiment in (c). Comparison of the EOR specific activity at 0.45 vs. RHE during the first forward scan (d), the corresponding potential to the low onset peak χ maximum (e), and the respective charge of peak χ (f) of the three $Pt_3Ni_1Rh_x$-oct/C octahedra.

and also suggests an earlier C–C bond break. These results indicate that the novel octahedral $Pt_3Ni_1Rh_x$-oct/C nanoparticle catalyst shows high catalytic activity for EOR in alkaline media. This behavior is plausibly explained by the ability of $Ni(OH)_x$ phases, which form on the surface facets of the Ni-containing bulk phases, to act as efficient oxygen-donating entities.[8b,10]

The stability of the electrocatalysts was investigated, as customary, using chronoamperometric measurements at $E =$ 0.45 V vs. RHE (Figure 2c). All of the $Pt_3Ni_1Rh_x$-oct/C electrocatalysts showed good durability in the EOR in alkaline media. The observed stationary activity after the initial current drop is in good agreement with the activity ranking of the electrocatalysts in the potentiodynamic measurements at the equivalent potential (Figure 2d). Studies on the PtNi-based catalytic system for the EOR are very sparse, however, the $Pt_3Ni_1Rh_x$-oct/C octahedral electrocatalysts all not only outperformed a binary PtNi EOR electrocatalyst[11] but also our corresponding spherical PtRhNi/C electrocatalysts,[5] indicating that the shape of the catalysts has a decisive influence on the catalytic properties of the surface site ensembles. In summary, all electrochemical results confirm that octahedral $Pt_3Ni_1Rh_x$-oct/C exhibits good catalytic performance towards the EOR and, therefore, offers great promise for applications in DEFCs in the future.

Even more interestingly, electrochemical investigation of the ethanol oxidation reaction on the octahedral $Pt_3Ni_1Rh_x$-oct/C surfaces revealed exceptionally low onset potential features near the reversible oxidation potential for ethanol oxidation (Figure 2b, $E^0_{Anode} \approx 0.08$ V vs. RHE, pH 14)[12] in the first forward scans (hereinafter: peak χ), which was not observed in similar investigations on spherical nanoparticle PtRhNi/C catalysts.[5] To the best of our knowledge, such low onset potentials for ethanol oxidation with such low overpotentials have not been reported to date. Although it already occurs in the $H_{UPD}$ region, it can be ruled out that peak χ originates from the underpotential deposition of hydrogen on the catalyst surface. This is because, in general, hydrogen features are inhibited on all catalysts that are active for the ethanol oxidation reaction due to the strong adsorption of ethanol molecules on the active sites.[13] Figure 2d–f summarizes the EOR activity at 0.45 V vs. RHE, the potential of the maximum of the onset feature in the first EOR scan, as well as the area under that feature. The first scan onset feature appears at earlier potentials and shows a higher corresponding area under the current density curve with higher amounts of Rh in the catalyst (PtNiRh-6/C > PtNiRh-3/C > PtNiRh-1/C). This behavior does not correlate directly with the overall EOR activity; the PtNiRh-3/C electrocatalyst shows the highest activity for the EOR, indicating a maximum for a certain atomic mixture of Pt, Ni and Rh on the surface.

The potential-dependent selectivity for this variety of organic products on EOR electrocatalysts can be studied using in situ Fourier transformation infrared attenuated total reflection(FTIR ATR) spectroscopy, however in situ FTIR studies for the EOR in alkaline media are sparse and often provide only insufficient comparability with electrochemical standard measurements.[3,12,14] We correlated activity with selectivity towards certain pathways of the EOR, by following the selectivity of the three $Pt_3Ni_1Rh_x$-oct/C electrocatalysts.

Figure 3 shows recorded spectra from all three catalysts during the first forward scan of ethanol oxidation in alkaline media. Carbon dioxide ($CO_2$), acetic acid ($CH_3COOH$) and acetaldehyde ($CH_3CHO$) are the potential products deriving from ethanol oxidation. According to previous studies, the bands at 2341 cm$^{-1}$ can be attributed to ν($CO_2$); ν(C=O) carbonyl vibration is responsible for the observed ≈1700 cm$^{-1}$ band stemming from either CHO or COOH; 1585 cm$^{-1}$ bands can be attributed to $\nu_s$(O-C-O) asymmetric stretching acetate; bands at 1381 cm$^{-1}$ can be attributed to for in-plane bending vibrations of the -$CH_3$ group of the adsorbed acetate δ($CH_3$) and at 1354 cm$^{-1}$ for adsorbed acetaldehyde, respectively.[12,14,15]

  

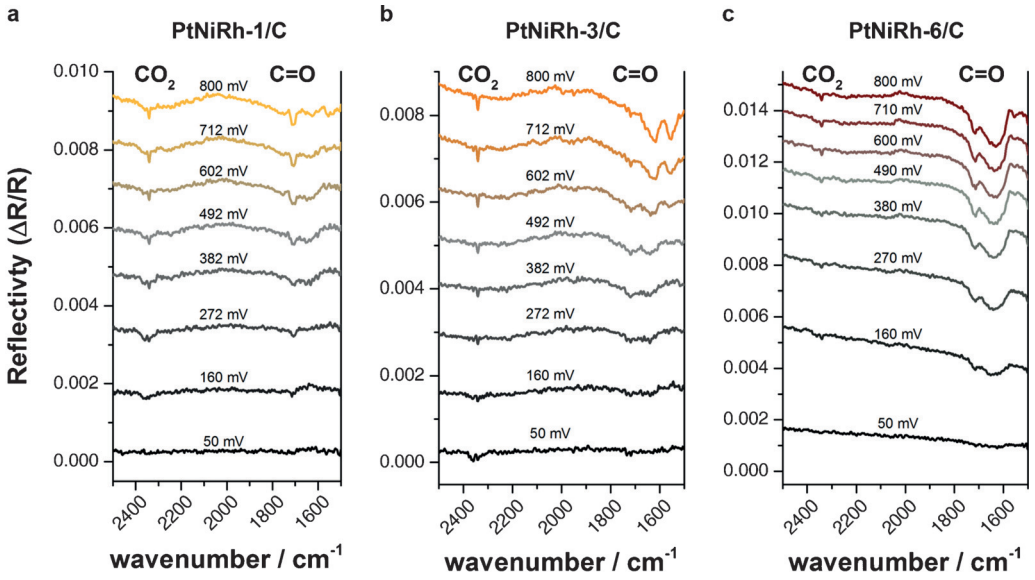


***Figure 3.*** In situ FTIR ATR spectra recorded during the EOR on a) PtNiRh-1/C, b) PtNiRh-3/C, and c) PtNiRh-6/C. 128 interferograms (resolution 4 $cm^{-1}$) were collected and combined for each spectrum. The working electrode potential ranges during the first linear sweep voltammetry with a scan rate of 1 $mV s^{-1}$ in 0.5 M EtOH in 0.1 M KOH are indicated in the figures.

It is generally accepted that the oxidation of ethanol proceeds via a dual pathway mechanism, as shown in Figure S5.[1c,14,16] Ethanol can be oxidized to $C_2$-structured acetaldehyde and subsequently to acetic acid, transferring only 4 electrons in the process. Acetic acid marks a "dead end" in the mechanism, since its further oxidation is very difficult under ambient conditions.[16i] Alternatively, the C–C bond can be broken in ethanol and also in acetaldehyde, yielding adsorbed single C species such as $CO_{ads}$ and $CH_{x,ads}$.[16j,17] These species can subsequently be oxidized to $CO_2$, yielding 12 electrons in total. The single $C_1$ adsorbates normally require a high overpotential to be oxidized,[16i,18] thereby reducing the overall efficiency of the reaction.

The integrated band intensities can therefore best be attributed to the two different pathways and are correlated in Figure 4 with the corresponding first in situ forward scan with 1 $mV s^{-1}$ in the electrochemical cell. PtNiRh-1/C shows a very low onset of $CO_2$ production only some band growth in the $C_2$ pathway region.

PtNiRh-6/C has a high onset potential for $CO_2$ but nearly instant production of $C_2$ pathway products, even at low potentials. The most active PtNiRh-3/C catalyst shows a low onset of $CO_2$, but not as high a rise in the band area as does the PtNiRh-1/C, while also showing a low onset for the production of $C_2$ pathway products. The lowest overall activity for the three electrocatalysts also corresponds with the absence of $CO_2$ band growth, as can be intuitively explained by the dominance of the 4 or 2 electron yield per molecule for this pathway, while complete oxidation yields 12 electrons per molecule. Interestingly, the higher selectivity towards the complete oxidation of PtNiRh-1/C alone cannot account for the highest overall activity; the highest current density yields correlate with surface active sites that can promote both reaction pathways, as in PtNiRh-3/C. Both PtNiRh-1/C and PtNiRh-3/C show $C_1$ pathway onset features between 0.3 and 0.4 V vs. RHE, while PtNiRh-6/C still shows only little oxidation towards $CO_2$. This behavior coincides with the microstructural observation of an already formed Rh-rich shell, which appears to inhibit complete oxidation by blocking important ternary surface site ensembles on the {111} facets that are capable of splitting ethanol effec-

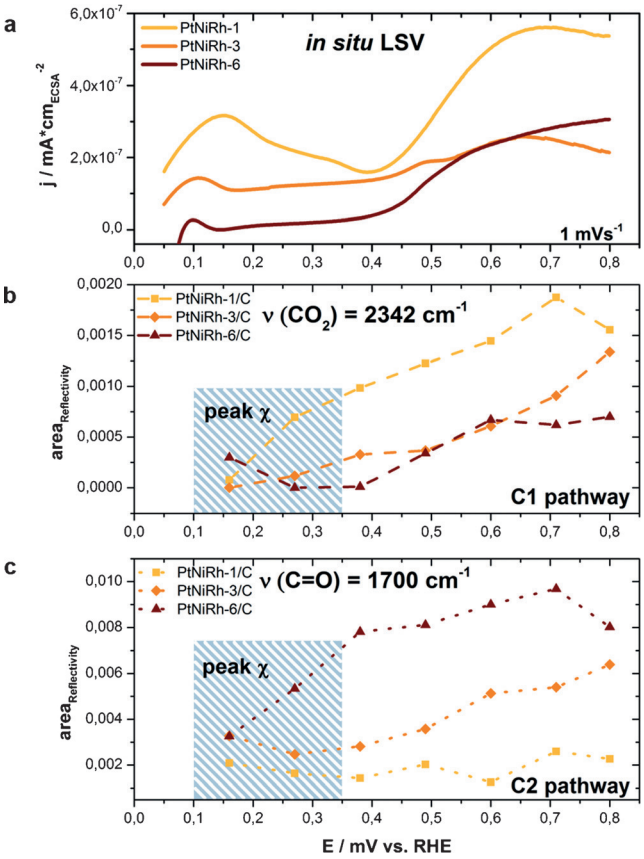


***Figure 4.*** a) First in situ linear sweep voltammetry scans and corresponding integrated in situ FTIR ATR band intensities of b) $CO_2$ (2342 $cm^{-1}$) and c) partial oxidation pathway for $CH_3CHO$ and $CH_3COOH$ (1700 $cm^{-1}$) of PtNiRh-oct/C electrocatalysts during the electrooxidation of ethanol. 128 interferograms (resolution 4 $cm^{-1}$) were collected and combined for each spectrum. The working electrode potential ranges during the first linear sweep voltammetry with a scan rate of 1 $mV s^{-1}$ in 0.5 M EtOH in 0.1 M KOH are indicated in the figures.

tively at such low overpotentials. Nevertheless, the Rh-rich shell provides a low onset for the oxidation of ethanol via the $C_2$ pathway. The presented FTIR data for PtNiRh-6/C is in agreement with Cuesta et al. who reported pioneering work of atomic ensemble effects for these type of reactions, showing that the absence of three contiguous Pt atoms on cyanide-modified Pt(111) surfaces lead to the blockage of the formation of adsorbed CO during oxidation reactions.[19]

In conclusion this work demonstrates the influence of surface site coordination and reported the successful synthesis of octahedral $Pt_3Ni_1Rh_x$-oct/C electrocatalysts with a designed variation in Rh percentage that leads to highly shape-controlled supported nanoparticles. All catalysts show a narrow edge length distribution and high crystallinity as well as good electrochemical activity and stability towards the oxidation of ethanol in alkaline media.

In situ FTIR studies reveal prevalence for the complete oxidation of ethanol via a $C_1$ pathway for the lowest Rh content, with well distributed ternary surface site ensembles on the octahedral {111} facets, while the $C_2$ pathway dominates for the catalyst with the highest Rh content and an already formed Rh shell. The overall specific activity peaks for PtNiRh-3/C are possibly due to the simultaneous occurrence of both reaction pathways. Our study strongly suggests that for a low Rh content, that is, before the formation of (PtNi alloy core)/(Rh shell) octahedra, different electronic effects compromising all three metal components prevails, resulting in the ability to break the C–C bond at low overpotentials near the reversible potential of the anodic complete oxidation of ethanol, which could not be achieved with existing catalysts.

## Acknowledgements

The project on which this report is based was supported by the Federal Ministry of Education and Research under the reference number 16N11929. Responsibility for the contents of this publication lies with the author. Partial financial support by the German Research Foundation (DFG) through grants STR 596/4-1 ("Pt stability") and STR 596/5-1 is gratefully acknowledged. We thank the Zentraleinrichtung für Elektronenmikroskopie (Zelmi) of the Technical University Berlin for their support with TEM. N.E., V.B. and P.S. thank Annette Wittebrock for RDE measurements. M.H. thanks the Deutsche Forschungsgemeinschaft (DFG) for support within the grant HE 7192/1-1.

## Conflict of interest

The authors declare no conflict of interest.

**Keywords:** electrocatalysis · ethanol oxidation · IR spectroscopy · octahedral nanoparticles · PtNiRh

**How to cite:** *Angew. Chem. Int. Ed.* **2017**, *56*, 6533–6538
*Angew. Chem.* **2017**, *129*, 6633–6638

[1] a) E. Antolini, *J. Power Sources* **2007**, *170*, 1–12; b) F. Vigier, C. Coutanceau, F. Hahn, E. M. Belgsir, C. Lamy, *J. Electroanal. Chem.* **2004**, *563*, 81–89; c) F. Colmati, G. Tremiliosi-Filho, E. R. Gonzalez, A. Berna, E. Herrero, J. M. Feliu, *Faraday Discuss.* **2009**, *140*, 379–397; d) A. Rabis, P. Rodriguez, T. J. Schmidt, *ACS Catal.* **2012**, *2*, 864–890; e) C. Lamy, S. Rousseau, E. M. Belgsir, C. Coutanceau, J. M. Léger, *Electrochim. Acta* **2004**, *49*, 3901–3908.

[2] W. Zhou, Z. Zhou, S. Song, W. Li, G. Sun, P. Tsiakaras, Q. Xin, *Appl. Catal. B* **2003**, *46*, 273–285.

[3] E. H. Fontes, R. M. Piasentin, J. M. S. Ayoub, J. C. M. da Silva, M. H. M. T. Assumpção, E. V. Spinacé, A. O. Neto, R. F. B. de Souza, *Mater. Renewable Sustainable Energy* **2015**, *4*, 3.

[4] a) N. Erini, R. Loukrakpam, V. Petkov, E. A. Baranova, R. Yang, D. Teschner, Y. Huang, S. R. Brankovic, P. Strasser, *ACS Catal.* **2014**, *4*, 1859–1867; b) N. Erini, P. Krause, M. Gliech, R. Yang, Y. Huang, P. Strasser, *J. Power Sources* **2015**, *294*, 299–304; c) M. Oezaslan, F. Hasché, P. Strasser, *J. Electrochem. Soc.* **2012**, *159*, B394–B405; d) F. Hasché, M. Oezaslan, P. Strasser, *ChemCatChem* **2011**, *3*, 1805–1813; e) Z. Liu, S. Koh, C. Yu, P. Strasser, *J. Electrochem. Soc.* **2007**, *154*, B1192–B1199; f) P. Strasser, *J. Comb. Chem.* **2008**, *10*, 216–224; g) C.-T. Hsieh, J.-Y. Lin, J.-L. Wei, *Int. J. Hydrogen Energy* **2009**, *34*, 685–693; h) M. Li, A. Kowal, K. Sasaki, N. Marinkovic, D. Su, E. Korach, P. Liu, R. R. Adzic, *Electrochim. Acta* **2010**, *55*, 4331–4338; i) N. Zhang, Y. Feng, X. Zhu, S. Guo, J. Guo, X. Huang, *Adv. Mater.* **2017**, *29*, 0.

[5] N. Erini, S. Rudi, V. Beermann, P. Krause, R. Yang, Y. Huang, P. Strasser, *ChemElectroChem* **2015**, *2*, 903–908.

[6] a) M. Oezaslan, F. Hasché, P. Strasser, *J. Phys. Chem. Lett.* **2013**, *4*, 3273–3291; b) V. Beermann, M. Gocyla, E. Willinger, S. Rudi, M. Heggen, R. E. Dunin-Borkowski, M.-G. Willinger, P. Strasser, *Nano Lett.* **2016**, *16*, 1719–1725; c) P. Strasser, *Science* **2015**, *349*, 379–380.

[7] C. Busó-Rogero, V. Grozovski, F. J. Vidal-Iglesias, J. Solla-Gullón, E. Herrero, J. M. Feliu, *J. Mater. Chem. A* **2013**, *1*, 7068–7076.

[8] a) L. Gan, C. Cui, M. Heggen, F. Dionigi, S. Rudi, P. Strasser, *Science* **2014**, *346*, 1502–1506; b) C. Cui, L. Gan, M. Heggen, S. Rudi, P. Strasser, *Nat. Mater.* **2013**, *12*, 765–771.

[9] C. Cui, L. Gan, H.-H. Li, S.-H. Yu, M. Heggen, P. Strasser, *Nano Lett.* **2012**, *12*, 5885–5889.

[10] a) C. Cui, M. Ahmadi, F. Behafarid, L. Gan, M. Neumann, M. Heggen, B. R. Cuenya, P. Strasser, *Faraday Discuss.* **2013**, *162*, 91–112; b) P. Novacek, P. Varga, *Surf. Sci.* **1991**, *248*, 183–192; c) P. B. Balbuena, D. Altomare, N. Vadlamani, S. Bingi, L. A. Agapito, J. M. Seminario, *J. Phys. Chem. A* **2004**, *108*, 6378–6384; d) R. Subbaraman, D. Tripkovic, D. Strmcnik, K.-C. Chang, M. Uchimura, A. P. Paulikas, V. Stamenkovic, N. M. Markovic, *Science* **2011**, *334*, 1256–1260.

[11] D. Soundararajan, J. H. Park, K. H. Kim, J. M. Ko, *Curr. Appl. Phys.* **2012**, *12*, 854–859.

[12] C. Busó-Rogero, E. Herrero, J. M. Feliu, *ChemPhysChem* **2014**, *15*, 2019–2028.

[13] T. Iwasita, X. H. Xia, H. D. Liess, W. Vielstich, *J. Phys. Chem. B* **1997**, *101*, 7542–7547.

[14] P. A. Christensen, S. W. M. Jones, A. Hamnett, *J. Phys. Chem. C* **2012**, *116*, 24681–24689.

[15] S. C. S. Lai, S. E. F. Kleijn, F. T. Z. Öztürk, V. C. van Rees Vellinga, J. Koning, P. Rodriguez, M. T. M. Koper, *Catal. Today* **2010**, *154*, 92–104.

[16] a) A. Kowal, M. Li, M. Shao, K. Sasaki, M. B. Vukmirovic, J. Zhang, N. S. Marinkovic, P. Liu, A. I. Frenkel, R. R. Adzic, *Nat. Mater.* **2009**, *8*, 325–330; b) T. Iwasita, E. Pastor, *Electrochim. Acta* **1994**, *39*, 531–537; c) M. C. Figueiredo, A. Santasalo-Aarnio, F. J. Vidal-Iglesias, J. Solla-Gullón, J. M. Feliu, K.

  

Kontturi, T. Kallio, *Appl. Catal. B* **2013**, *140 – 141*, 378 – 385; d) V. Rao, Hariyanto, C. Cremers, U. Stimming, *Fuel Cells* **2007**, *7*, 417 – 423; e) M. H. Shao, R. R. Adzic, *Electrochim. Acta* **2005**, *50*, 2415 – 2422; f) I. Kim, O. H. Han, S. A. Chae, Y. Paik, S.-H. Kwon, K.-S. Lee, Y.-E. Sung, H. Kim, *Angew. Chem. Int. Ed.* **2011**, *50*, 2270 – 2274; *Angew. Chem.* **2011**, *123*, 2318 – 2322; g) M. Li, P. Liu, R. R. Adzic, *J. Phys. Chem. Lett.* **2012**, *3*, 3480 – 3485; h) S. C. S. Lai, M. T. M. Koper, *Phys. Chem. Chem. Phys.* **2009**, *11*, 10446 – 10456; i) S. C. S. Lai, M. T. M. Koper, *Faraday Discuss.* **2009**, *140*, 399 – 416; j) J. Shin, W. J. Tornquist, C. Korzeniewski, C. S. Hoaglund, *Surf. Sci.* **1996**, *364*, 122 – 130; k) U. Schmiemann, U. Müller, H. Baltruschat, *Electrochim. Acta* **1995**, *40*, 99 – 107; l) M. Heinen, Z. Jusys, R. J. Behm, *ECS Trans.* **2009**, *25*, 259 – 269; m) M. Heinen, Z. Jusys, R. J. Behm, *J. Phys. Chem. C* **2010**, *114*, 9850 – 9864.

[17] S. C. S. Lai, S. E. F. Kleyn, V. Rosca, M. T. M. Koper, *J. Phys. Chem. C* **2008**, *112*, 19080 – 19087.

[18] S. C. Chang, L. W. H. Leung, M. J. Weaver, *J. Phys. Chem.* **1990**, *94*, 6013 – 6021.

[19] a) A. Cuesta, M. Escudero, B. Lanova, H. Baltruschat, *Langmuir* **2009**, *25*, 6500 – 6507; b) A. Cuesta, *J. Am. Chem. Soc.* **2006**, *128*, 13332 – 13333.

Manuscript received: March 4, 2017
Version of record online: April 28, 2017

  